A database of flow and near pressure field signals obtained for subsonic and supersonic free jets using large-eddy simulations

Christophe Bogey*
CNRS, Ecole Centrale de Lyon, INSA Lyon, Universite Claude Bernard Lyon I,
Laboratoire de Mécanique des Fluides et d'Acoustique, UMR 5509, 69130 Ecully, France

(Updated on June 9, 2024)

The time signals obtained in the flow and near pressure fields of subsonic and supersonic free jets computed by highly-resolved compressible large-eddy simulations (LES) using cylindrical coordinates have been stored in a database. They can be shared with other researchers, upon request by email, to investigate, for instance, the development of turbulent structures and noise generation mechanisms in high-speed jets. The jet conditions (Mach and Reynolds numbers, temperature) and nozzle-exit boundary-layer characteristics (thickness, velocity profile, fluctuation level), the LES grid parameters and the recorded signals (nature and location of the variables stored, time duration and sampling frequency) are briefly described.

I. Nozzle-exit jet flow conditions

A. Isothermal jets at a Mach number of 0.9 at low and high Reynolds numbers

At first, two isothermal jets at a Mach number $\mathrm{M} = u_j/c_0 = 0.9$ at diameter-based Reynolds numbers $\mathrm{Re}_D = u_j D/\nu = 3125$ and $\mathrm{Re}_D = 10^5$ [1], where u_j, $D = 2r_0$, c_0 and ν are the jet nozzle-exit velocity and diameter, the speed of sound in the ambient medium and the kinematic molecular viscosity, have been simulated using LES. They are represented by a red diamond and a red bullet in figure 1. Their initial conditions are given in table 1. The parameters of the simulations and flow and noise properties of the jets are detailed in recent papers [2–6]. More results can also be found in references [7–12]. The mesh grid used for the LES of the two jets are referred to as CGz75a and FGz40 and are described in section II. The sets of files recorded in the two cases, named D2 and D0, are presented in section III. The recording times T are equal to $5,000 r_0/u_j$ and $5,250 r_0/u_j$.

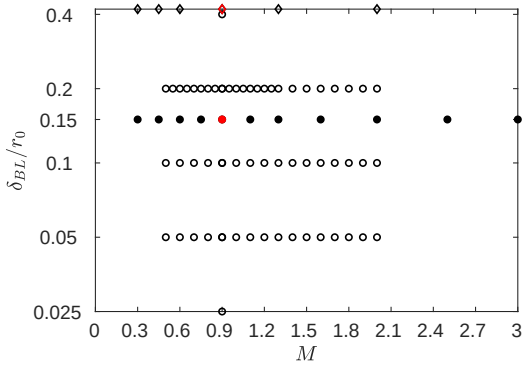

Fig. 1 Jets at $\mathrm{Re}_D = 10^5$ with • tripped and ∘ untripped boundary layers, and ⋄ at $\mathrm{Re}_D = 3125$: Mach number M and thickness δ_{BL} of the Blasius profiles at the pipe-nozzle inlet; ⋄ M09Re3125TaLd0420v1 and • M09Re1e5TaLd0150v9.

B. Low-Reynolds-number isothermal jets

On the basis of the simulation of the low-Reynolds-number jet M09Re3125TaLd0420v1 at $\mathrm{M} = 0.9$ and $\mathrm{Re}_D = 3,125$, isothermal jets also at $\mathrm{Re}_D = 3125$ but at $\mathrm{M} = 0.3$, 0.45, 0.6, 1.3 and 2, with peak turbulence intensities at the

*CNRS Research Scientist, christophe.bogey@ec-lyon.fr, ORCID iD: https://orcid.org/0000-0003-3243-747X

nozzle exit of $u'_e/u_j = 0.01$ for M $\leq$ 1.3 and 0.025 for M = 2, have been computed. They are collected in table 2, and represented by diamonds in figure 1.

C. High-Reynolds-number isothermal jets with untripped boundary layers

Isothermal jets at a Reynolds number $\mathrm{Re}_D = 10^5$ with untripped boundary layers have been considered in order to investigate the flow and sound fields of initially fully laminar jets. They are represented by circles in figure 1. The simulations of such jets is cheaper than those of jets with tripped boundary layers, allowing us to perform parametric studies at a reasonable cost.

1. Isothermal jets at a Mach number of 0.9 with different boundary-layers thicknesses

Isothermal jets at M = 0.9 and $\mathrm{Re}_D = 10^5$ with untripped boundary layers of different thicknesses [13] between $\delta_{BL} = 0.025r_0$ and $\delta_{BL} = 0.4r_0$ have been computed by LES. They are defined in table 3. Results of the simulations are presented in several papers [2, 4–6, 14].

2. Isothermal jets at Mach numbers between 0.5 and 2

Isothermal jets with untripped boundary-layers of thicknesses $\delta_{BL} = 0.05r_0$, $0.1r_0$ and $0.2r_0$ at Mach numbers varying between 0.5 and 2 in increments of 0.05 or 0.1 have been computed. They are defined in table 4. Results of the simulations are presented in two papers [4, 14].

3. Hot jets at Mach numbers between 0.5 and 2

Hot jets with untripped boundary-layers of thickness $\delta_{BL} = 0.1r_0$ at temperature $T_j = 1.5T_a$ or $T_j = 2.25T_a$, where T_a is the ambient temperature, at Mach numbers varying between 0.5 and 2 in increments of 0.05 or 0.1 have been computed [15]. They are defined in table 4.

D. High-Reynolds-number isothermal jets with tripped boundary-layers

Isothermal jets at $\mathrm{Re}_D = 10^5$ with tripped boundary-layers have been considered in order to investigate the flow and sound fields of initially highly disturbed jets. They are characterized by peak turbulence intensity u'_e/u_j typically of 9% at the nozzle exit.

1. Isothermal jets with nozzle-exit turbulence levels between 0 and 15%

Isothermal jets at M = 0.9 and $\mathrm{Re}_D = 10^5$ with peak turbulence intensity at the nozzle exit of $u'_e/u_j = 0$, 3%, 6%, 9%, 12% and 15% have been computed to study the effects of the upstream turbulence levels [1, 16, 17]. They are defined in table 6.

2. Isothermal jets at Reynolds numbers between 12,500 and 400,000

Isothermal jets at M = 0.9 with highly disturbed nozzle-exit boundary layers with $u'_e/u_j \simeq 9\%$ have been computed for Reynolds numbers Re_D varying between $12,500$ and $400,000$ [18] to examine the Reynolds number effects. They are presented in table 7.

3. Isothermal jets with different boundary-layer thicknesses

Isothermal jets at M = 0.9 and $\mathrm{Re}_D \simeq 50,000$ with highly disturbed boundary layers of different thicknesses between $\delta_{BL} = 0.09r_0$ and $0.42r_0$ have been computed [19]. They are reported in table 8. Results are available in a recent paper [20].

4. Isothermal jets at Mach numbers between 0.3 and 3

On the basis of the simulation of the jet M09Re1e5TaLd0150v9 at M = 0.9 and $\mathrm{Re}_D = 100,000$ with $u'_e/u_j = 9\%$, isothermal jets also with $\mathrm{Re}_D = 100,000$ and $u'_e/u_j = 9\%$ but at M = 0.3, 0.45, 0.6, 0.75, 1.1, 1.3, 1.6, 2, 2.5 and 3

have been computed. They are collected in table 9, and are represented by bullets in figure 1. The parameters of the simulations and the flow and noise properties of the jets at M = 0.6, 0.75, 1.1, 1.3 and 2 are presented in very recent papers [4, 5, 14].

5. Isothermal jets with thick nozzle lips

Isothermal jets at M = 0.6, 0.9 and 1.3, $\mathrm{Re}_D = 100,000$ with $u'_e/u_j = 9\%$, as the jets M06Re1e5TaLd0150v9, M09Re1e5TaLd0150v9 and M13Re1e5TaLd0150v9 have been simulated [21]. In these case, the nozzle lip is 16 thicker than previously ($\delta_{lip} = 0.93r_0$ instead of $\delta_{lip} = 0.05r_0$). They are collected in table 10.

6. Isothermal jets with non-laminar boundary-layer profiles

Isothermal jets at M = 0.9 and $\mathrm{Re}_D = 50,000$ with highly disturbed boundary layers ($u'_e/u_j = 6\%$ or 9%) of different shapes (L: laminar Blasius profile; T1, T2 and T3: transitional and turbulent profiles) [22] have been computed. They are defined in table 11. The parameters of the simulations and the flow and noise properties of the jets are presented in references [20, 23].

7. Hot jets at a Mach number of 0.9

Hot jets at a Mach number of M = 0.9 and Reynolds numbers Re_D between 25,000 and 200,000 with highly disturbed boundary layers ($u'_e/u_j = 9\%$) have been computed [15, 24–26]. Their nozzle-exit static temperatures are $T_j = 1.5T_a$ or $T_j = 2.25T_a$, where T_a is the ambient temperature. They are defined in table 12.

8. Hot jets at Mach numbers between 0.45 and 1.6

Hot jets at $\mathrm{Re}_D = 100,000$ and at M = 0.45, 0.6, 0.75, 1.1, 1.3 and 1.6 with highly disturbed boundary layers ($u'_e/u_j = 9\%$) have been computed [15]. As for the hot jets at M = 0.9, their nozzle-exit static temperatures are equal to $T_j = 1.5T_a$ or $T_j = 2.25T_a$. They are defined in table 13.

9. Rocket jets at Mach numbers 3

Finally, in addition to the isothermal jet at Mach 3 reported in table 9, two other rocket-type jets have been computed. The first one is a perfectly expanded cold jet at $\mathrm{M}_j = 3$ (i.e. $\mathrm{M}_a = 1.77$) and $Re_D = 200,000$, considered in a work to investigate wave steepening and shock coalescence in the near field of high-speed jets [27, 28]. The second one is an over-expanded hot jet at an exhaust Mach number $\mathrm{M}_e = 3.1$ and $Re_D = 200,000$, with an exhaust temperature $T_e = 738$ K, considered in studies of rocket jets impinging on full or perforated plates [29, 30] (the jet has an ideally expanded Mach number $\mathrm{M}_j = 2.9$ and an acoustic Mach number $\mathrm{M}_a = 4.9$).

II. Mesh grid parameters

Some characteristics of the mesh grids CGXX and FGXX used for the simulations in the radial and axial directions, namely the numbers of points, the grid physical extents and the mesh spacings at specific positions, are provided in table 14. The CG (coarse) and FG (fine) grids are employed for the jets at $\mathrm{Re}_D = 3,125$ and $\mathrm{Re}_D \geq 12,500$, respectively, and XX indicates that the grid extends down to $z = L_z = XXr_0$ in the axial direction, excluding the outflow sponge zone. The grids are detailed in recent papers [2–4, 14]. In particular, a grid sensitivity study has been conducted in reference [2] to assess the quality of the FGz40 grid for the LES of the high Reynolds number tripped jet M09Re1e5TaLd0150v9. The numbers of points n_θ in the azimuth (256, 512 or 1024) in the different simulations, depending on the thickness and state of the nozzle-exit boundary layer, are given in tables 1-12. For illustration purposes, the variations of the radial and axial mesh spacings in FGz40, FGz50 and FGz60 are shown in figure 2.

III. Recording files

The recording files (nature and location of the variables stored, time durations and sampling frequencies) are defined in table 15 Three-dimensional fields are stored in the 3Dxxx files, and two-dimensional fields at constant radial, azimuthal and axial positions are stored in the Rxx, Txx and Zxx files, respectively. The maximum Strouhal number

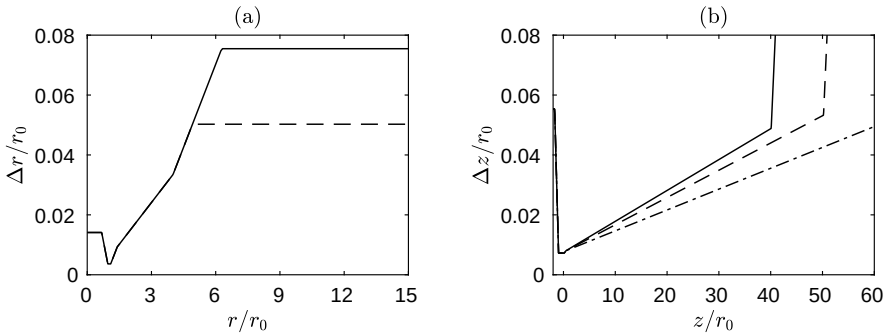

Fig. 2 Variations (a) of radial mesh spacing Δr for ——— FGz40 and − − − FGz50 and FGz60 and (b) of axial mesh spacing Δz for ——— FGz40, − − − FGz50 and − · − · FGz60.

$\mathrm{St}_D = fD/u_j$, where f is the frequency, allowed by the sampling frequency is equal to 32 for T_{HF} and to 6.4 or 12.8 in the other cases.

The sets of files recorded in the different simulations, referred to as D0, D1, D2 and D3 in tables 1-12, are defined in table 16. For storage issues, all the files are saved (case D0) only for the isothermal tripped jet at Mach 0.9 and Reynolds 100,000 (M09Re1e5TaLd0150v9). For most other jets at high Reynolds numbers, the 3-D fields and the 2-D fields at $\theta = \pi/4 \longrightarrow 13\pi/4$ every $\pi/2$ are not stored (case D1). For the jets at Reynolds 3,125, in addition, the Fourier coefficients for $n_{\theta=5-8}$ are not recorded (case D2). Finally, case D3 applies to the untripped jets at M $\neq$ 0.9.

Acknowledgments

The simulations have been performed using the HPC resources of PMCS2I (Pôle de Modélisation et de Calcul en Sciences de l'Ingénieur et de l'Information) of Ecole Centrale de Lyon, PSMN (Pôle Scientifique de Modélisation Numérique) of ENS de Lyon and P2CHPD (Pôle de Calcul Hautes Performances Dédiés) of Université Lyon I, and the resources of CINES (Centre Informatique National de l'Enseignement Supérieur), IDRIS (Institut du Développement et des Ressources en Informatique Scientifique) and TGCC (Très Grand Centre de calcul du CEA) under the allocations made by GENCI (Grand Equipement National de Calcul Intensif).

References

[1] Bogey, C., Marsden, O., and Bailly, C., "Large-Eddy Simulation of the flow and acoustic fields of a Reynolds number 10^5 subsonic jet with tripped exit boundary layers," *Phys. Fluids*, Vol. 23, No. 3, 2011, p. 035104. https://doi.org/10.1063/1.3555634.

[2] Bogey, C., "Grid sensitivity of flow field and noise of high-Reynolds-number jets computed by large-eddy simulation," *Int. J. Aeroacoust.*, Vol. 17, No. 4-5, 2018, pp. 399–424. https://doi.org/10.1177/1475472X18778287.

[3] Bogey, C., "Two-dimensional features of correlations in the flow and near pressure fields of Mach number 0.9 jets," Tech. Rep. 2019-0806, AIAA Paper, 2019. https://doi.org/10.2514/6.2019-0806.

[4] Bogey, C., "Acoustic tones in the near-nozzle region of jets: characteristics and variations between Mach numbers 0.5 and 2," *J. Fluid Mech.*, Vol. 921, 2021, p. A3. https://doi.org/10.1017/jfm.2021.426.

[5] Bogey, C., "Tones in the acoustic far field of jets in the upstream direction," *AIAA J.*, Vol. 60, No. 4, 2022, pp. 2397–2406. https://doi.org/10.2514/1.J061013.

[6] Bogey, C., "Effects of the upstream-propagating guided jet waves on the mixing layers of Mach number 0.9 free jets," Tech. Rep. 2022-2870, AIAA Paper, 2022. https://doi.org/10.2514/6.2022-2870.

[7] Camussi, R., and Bogey, C., "Intermittent statistics of the 0-mode pressure fluctuations in the near field of Mach 0.9 circular jets at low and high Reynolds numbers," *Theor. Comput. Fluid Dyn.*, Vol. 35, No. 2, 2021, pp. 229–247. https://doi.org/10.1007/s00162-020-00553-9.

[8] Micci, G., Camussi, R., Meloni, S., and Bogey, C., "Intermittency and stochastic modeling of low- and high-Reynolds-number compressible jets," *AIAA J.*, Vol. 60, No. 3, 2022, pp. 1983–1990. https://doi.org/10.2514/1.J061128.

[9] Adam, A., Papamoschou, D., and Bogey, C., "Imprint of vortical structures on the near-field pressure of a turbulent jet," *AIAA J.*, Vol. 60, No. 3, 2022, pp. 1578–1591. https://doi.org/10.2514/1.J061010.

[10] Camussi, R., Meloni, S., and Bogey, C., "On the influence of the nozzle exhaust initial conditions on the near field acoustic pressure," *Acta Acust.*, Vol. 6, No. 57, 2022, pp. 1–9. https://doi.org/10.1051/aacus/2022051.

[11] Palma, G., Meloni, S., Camussi, R., Iemma, U., and Bogey, C., "Data-driven multiobjective optimization of wave packets for near-field subsonic jet noise," *AIAA J.*, Vol. 61, No. 5, 2023, pp. 2179–2188. https://doi.org/10.2514/1.J062261.

[12] Spieser, E., Bogey, C., and Bailly, C., "Noise predictions of a Mach 0.9 round jet using tailored adjoint Green's functionse," *J. Sound Vib.*, Vol. 548, No. 117532, 2023, pp. 1–24. https://doi.org/10.1016/j.jsv.2022.117532.

[13] Bogey, C., and Bailly, C., "Influence of nozzle-exit boundary-layer conditions on the flow and acoustic fields of initially laminar jets," *J. Fluid Mech.*, Vol. 663, 2010, pp. 507–539. https://doi.org/10.1017/S0022112010003605.

[14] Bogey, C., "Interactions between upstream-propagating guided jet waves and shear-layer instability waves near the nozzle of subsonic and nearly ideally expanded supersonic free jets with laminar boundary layers," *J. Fluid Mech.*, Vol. 949, 2022, p. A41. https://doi.org/10.1017/jfm.2022.776.

[15] Bogey, C., "Properties of the tones emerging in the near-field pressure spectra of hot high-speed jets," Tech. Rep. 2024-3031, AIAA Paper, 2024. https://doi.org/10.2514/6.2024-3031.

[16] Bogey, C., Marsden, O., and Bailly, C., "On the spectra of nozzle-exit velocity disturbances in initially nominally turbulent, transitional jets," *Phys. Fluids*, Vol. 23, No. 9, 2011, p. 091702. https://doi.org/10.1063/1.3642642.

[17] Bogey, C., Marsden, O., and Bailly, C., "Influence of initial turbulence level on the flow and sound fields of a subsonic jet at a diameter-based Reynolds number of 10^5," *J. Fluid Mech.*, Vol. 701, 2012, pp. 352–385. https://doi.org/10.1017/jfm.2012.162.

[18] Bogey, C., Marsden, O., and Bailly, C., "Effects of moderate Reynolds numbers on subsonic round jets with highly disturbed nozzle-exit boundary layers," *Phys. Fluids*, Vol. 24, No. 10, 2012, p. 105107. https://doi.org/10.1063/1.4757667.

[19] Bogey, C., and Marsden, O., "Identification of the effects of the nozzle-exit boundary-layer thickness and its corresponding Reynolds number in initially highly disturbed subsonic jets," *Phys. Fluids*, Vol. 25, No. 5, 2013, p. 055106. https://doi.org/10.1063/1.4807071.

[20] Bogey, C., "Generation of excess noise by jets with highly disturbed laminar boundary-layer profiles," *AIAA J.*, Vol. 59, No. 2, 2021, pp. 569–579. https://doi.org/10.2514/1.J059610.

[21] Bogey, C., "Effects of nozzle-lip thickness on the tones in the near-field pressure spectra of high-speed jets,," Tech. Rep. 2023-3935, AIAA Paper, 2023. https://doi.org/10.2514/6.2023-3935.

[22] Bogey, C., and Marsden, O., "Influence of nozzle-exit boundary-layer profile on high-subsonic jets," Tech. Rep. 2014-2600, AIAA Paper, 2014. https://doi.org/10.2514/6.2014-2600.

[23] Bogey, C., and Sabatini, R., "Effects of nozzle-exit boundary-layer profile on the initial shear-layer instability, flow field and noise of subsonic jets," *J. Fluid Mech.*, Vol. 876, 2019, pp. 288–325. https://doi.org/10.1017/jfm.2019.546.

[24] Bogey, C., and Marsden, O., "Numerical investigation of temperature effects on properties of subsonic turbulent jets," Tech. Rep. 2013-2140, AIAA Paper, 2013. https://doi.org/10.2514/6.2013-2140.

[25] Bogey, C., "A study of the effects of temperature on velocity and density fluctuations in high-subsonic jets," Tech. Rep. 2014-0524, AIAA Paper, 2014. https://doi.org/10.2514/6.2014-0524.

[26] Martin-Martin, L., Bogey, C., Clair, V., and Gabard, G., "Computational study on sound scattering by jet shear layers," Tech. Rep. 2024-3031, AIAA Paper, 2024. https://doi.org/10.2514/6.2024-3183.

[27] Pineau, P., and Bogey, C., "Numerical investigation of wave steepening and shock coalescence near a cold Mach 3 jet," *J. Acoust. Soc. Am.*, Vol. 149, No. 1, 2021, pp. 357–370. https://doi.org/10.1121/10.0003343.

[28] Willis, W. A., Valdez, J. A., Pineau, P., Bogey, C., Tinney, C. E., and Hamilton, M. F., "A study of Mach wave coalescence using spark sources and large-eddy simulation," Tech. Rep. 2023-0021, AIAA Paper, 2023. https://doi.org/10.2514/6.2023-0021.

[29] Varé, M., and Bogey, C., "Flow and acoustic fields of rocket jets impinging on a perforated plate," *AIAA J.*, Vol. 60, No. 8, 2022, pp. 4614–4627. https://doi.org/10.2514/1.J061253.

[30] Varé, M., and Bogey, C., "Presence and properties of acoustic peaks near the nozzle of a rocket jet impinging on a plate," *Acta Acust.*, Vol. 6, 2022, p. 36. https://doi.org/10.1051/aacus/2022033.

Table 1 Mach and Reynolds numbers M and Re_D, jet temperature T_j, shape (L: laminar Blasius profile, T: transitional or turbulent profile) and thickness δ_{BL} of the boundary-layer profile imposed at the pipe nozzle inlet, peak turbulence intensity u'_e/u_j at the nozzle exit, grid used, number of points n_θ in the azimuthal direction, simulation time T after the transient period and recording files.

jet	M	Re_D	T_j/T_a	BL	δ_{BL}/r_0	u'_e/u_j	grid	n_θ	Tu_j/r_0	data
M09Re3125TaLd0420v1	0.9	3,125	1	L	0.42	1%	CGz75	512	5,000	D2
M09Re1e5TaLd0150v9	0.9	100,000	1	L	0.15	9%	FGz40	1,024	5,500	D0

Table 2 LES of low-Reynolds-number isothermal jets; see caption of table 1 for the different parameters.

jet	M	Re_D	T_j/T_a	BL	δ_{BL}/r_0	u'_e/u_j	grid	n_θ	Tu_j/r_0	data
M03Re3125TaLd0420v1	0.3	3,125	1	L	0.42	1%	CGz75a	512	1,000	D2
M045Re3125TaLd0420v1	0.45	3,125	1	L	0.42	1%	CGz75a	512	1,500	D2
M06Re3125TaLd0420v1	0.6	3,125	1	L	0.42	1%	CGz75a	512	4,000	D2
M09Re3125TaLd0420v1	0.9	3,125	1	L	0.42	1%	CGz75a	512	5,000	D2
M13Re3125TaLd0420v1	1.3	3,125	1	L	0.42	1%	CGz75b	512	4,000	D2
M2Re3125TaLd0420v2_5	2	3,125	1	L	0.42	2.5%	CGz90	512	3,000	D2

Table 3 LES of untripped isothermal jets at a Mach number of 0.9; see caption of table 1 for the different parameters.

jet	M	Re_D	T_j/T_a	L	δ_{BL}/r_0	u'_e/u_j	grid	n_θ	Tu_j/r_0	data
M09Re1e5TaLd0400v0	0.9	100,000	1	L	0.4	0%	FGz40	256	500	D1
M09Re1e5TaLd0200v0	0.9	100,000	1	L	0.2	0%	FGz40	256	3,000	D1
M09Re1e5TaLd0100v0	0.9	100,000	1	L	0.1	0%	FGz40	512	1,000	D1
M09Re1e5TaLd0050v0	0.9	100,000	1	L	0.05	0%	FGz40	512	1,000	D1
M09Re1e5TaLd0025v0	0.9	100,000	1	L	0.025	0%	FGz40	512	2,000	D1

Table 4 LES of untripped isothermal jets at Mach numbers between 0.5 and 2; see caption of table 1 for the different parameters.

jet	M	Re_D	T_j/T_a	L	δ_{BL}/r_0	u'_e/u_j	grid	n_θ	Tu_j/r_0	data
MxxxRe1e5TaLd0200v0	$0.5 \rightarrow 2$	100,000	1	L	0.2	0%	FGz40	256	500	D3
MxxxRe1e5TaLd0100v0	$0.5 \rightarrow 2$	100,000	1	L	0.1	0%	FGz40	256	500	D3
MxxxRe1e5TaLd0050v0	$0.5 \rightarrow 2$	100,000	1	L	0.05	0%	FGz40	256	500	D3

Table 5 LES of untripped hot jets at Mach numbers between 0.5 and 2; see caption of table 1 for the different parameters.

jet	M	Re_D	T_j/T_a	L	δ_{BL}/r_0	u'_e/u_j	grid	n_θ	Tu_j/r_0	data
MxxxRe1e5TaL1_5d0050v0	$0.5 \rightarrow 2$	100,000	1.5	L	0.05	0%	FGz40	256	500	D3
MxxxRe1e5TaL2_25d0050v0	$0.5 \rightarrow 2$	100,000	2.25	L	0.05	0%	FGz40	256	500	D3

Table 6 LES of tripped isothermal jets at M = 0.9; see caption of table 1 for the different parameters.

jet	M	Re_D	T_j/T_a	BL	δ_{BL}/r_0	u'_e/u_j	grid	n_θ	Tu_j/r_0	data
M09Re1e5TaLd0150v0	0.9	100,000	1	L	0.15	0%	FGz40	512	500	D1
M09Re1e5TaLd0150v3	0.9	100,000	1	L	0.15	3%	FGz40	1,024	500	D1
M09Re1e5TaLd0150v6	0.9	100,000	1	L	0.15	6%	FGz40	1,024	500	D1
M09Re1e5TaLd0150v9	0.9	100,000	1	L	0.15	9%	FGz40	1,024	5,500	D0
M09Re1e5TaLd0150v12	0.9	100,000	1	L	0.15	12%	FGz40	1,024	500	D1
M09Re1e5TaLd0150v15	0.9	100,000	1	L	0.15	15%	FGz40	1,024	500	D1

Table 7 LES of tripped isothermal jets at Reynolds numbers between 12,500 and 400,000; see caption of table 1 for the different parameters.

jet	M	Re_D	T_j/T_a	BL	δ_{BL}/r_0	u'_e/u_j	grid	n_θ	Tu_j/r_0	data
M09Re1_25e4TaLd0150v7_5	0.9	12,500	1	L	0.15	7.5%	FGz40	1,024	500	D1
M09Re2_5e4TaLd0150v9	0.9	25,000	1	L	0.15	9%	FGz40	1,024	500	D1
M09Re5e4TaLd0150v9	0.9	50,000	1	L	0.15	9%	FGz40	1,024	500	D1
M09Re1e5TaLd0150v9	0.9	100,000	1	L	0.15	9%	FGz40	1,024	5,500	D0
M09Re2e5TaLd0150v9	0.9	200,000	1	L	0.15	9%	FGz40	1,024	500	D1
M09Re4e5TaLd0150v9	0.9	400,000	1	L	0.15	9%	FGz40	1,024	500	D1

Table 8 LES of isothermal tripped jets with different boundary-layer thicknesses; see caption of table 1 for the different parameters.

jet	M	Re_D	T_j/T_a	L	δ_{BL}/r_0	u'_e/u_j	grid	n_θ	Tu_j/r_0	data
M09Re5e4TaLd0150v9	0.9	50,000	1	L	0.15	9%	FGz40	1,024	500	D1
M09Re5e4TaLd0090v9	0.9	50,000	1	L	0.09	9%	FGz40	1,024	500	D1
M09Re5e4TaLd0250v9	0.9	50,000	1	L	0.25	9%	FGz40	1,024	500	D1
M09Re5e4TaLd0420v9	0.9	50,000	1	L	0.42	9%	FGz40	1,024	500	D1
M09Re8_3e4TaLd0250v9	0.9	83,333	1	L	0.09	9%	FGz40	1,024	500	D1
M09Re3e4TaLd0250v9	0.9	30,000	1	L	0.25	9%	FGz40	1,024	500	D1
M09Re1_8e4TaLd0250v9	0.9	18,000	1	L	0.42	9%	FGz40	1,024	500	D1

Table 9 LES of isothermal tripped jets at Mach numbers between 0.3 and 3; see caption of table 1 for the different parameters.

jet	M	Re_D	T_j/T_a	BL	δ_{BL}/r_0	u'_e/u_j	grid	n_θ	Tu_j/r_0	data
M03Re1e5TaLd0150v9	0.3	100,000	1	L	0.15	9%	FGz40	1,024	1,200	D1
M045Re1e5TaLd0150v9	0.45	100,000	1	L	0.15	9%	FGz40	1,024	1,800	D1
M06Re1e5TaLd0150v9	0.6	100,000	1	L	0.15	9%	FGz40	1,024	4,250	D1
M075Re1e5TaLd0150v9	0.75	100,000	1	L	0.15	9%	FGz40	1,024	4,250	D1
M09Re1e5TaLd0150v9	0.9	100,000	1	L	0.15	9%	FGz40	1,024	5,500	D0
M11Re1e5TaLd0150v9	1.1	100,000	1	L	0.15	9%	FGz40	1,024	4,250	D1
M13Re1e5TaLd0150v9	1.3	100,000	1	L	0.15	9%	FGz50	1,024	3,000	D1
M16Re1e5TaLd0150v9	1.6	100,000	1	L	0.15	9%	FGz50	1,024	1,400	D1
M2Re1e5TaLd0150v9	2	100,000	1	L	0.15	9%	FGz60	1,024	3,000	D1
M25Re1e5TaLd0150v9	2.5	100,000	1	L	0.15	9%	FGz60	1,024	1,000	D1
M3Re1e5TaLd0150v9	3	100,000	1	L	0.15	9%	FGz70	1,024	1,800	D1

Table 10 LES of isothermal tripped jets at Mach numbers 0.6, 0.9 and 1.3 with thick nozzle lips; see caption of table 1 for the different parameters.

jet	M	Re_D	T_j/T_a	BL	δ_{BL}/r_0	u'_e/u_j	grid	n_θ	Tu_j/r_0	data
M06Re1e5TaLd0150v9Lip	0.6	100,000	1	L	0.15	9%	FGz40	1,024	1,000	D1
M09Re1e5TaLd0150v9Lip	0.9	100,000	1	L	0.15	9%	FGz40	1,024	1,000	D0
M13Re1e5TaLd0150v9Lip	1.3	100,000	1	L	0.15	9%	FGz50	1,024	1,000	D1

Table 11 LES of isothermal tripped jets with non-laminar boundary-layer profiles; see caption of table 1 for the different parameters.

jet	M	Re_D	T_j/T_a	BL	δ_{BL}/r_0	u'_e/u_j	grid	n_θ	Tu_j/r_0	data
M09Re5e4TaLd0250v0	0.9	50,000	1	L	0.25	0%	FGz40	1,024	500	D1
M09Re5e4TaT1d0250v0	0.9	50,000	1	T1	0.25	0%	FGz40	1,024	500	D1
M09Re5e4TaT2d0250v0	0.9	50,000	1	T2	0.25	0%	FGz40	1,024	500	D1
M09Re5e4TaT3d0250v0	0.9	50,000	1	T3	0.25	0%	FGz40	1,024	500	D1
M09Re5e4TaLd0250v6	0.9	50,000	1	L	0.25	6%	FGz40	1,024	500	D1
M09Re5e4TaT1d0250v6	0.9	50,000	1	T1	0.25	6%	FGz40	1,024	500	D1
M09Re5e4TaT2d0250v6	0.9	50,000	1	T2	0.25	6%	FGz40	1,024	500	D1

Table 12 LES of hot tripped jets at a Mach number of 0.9; see caption of table 1 for the different parameters.

jet	M	Re_D	T_j/T_a	BL	δ_{BL}/r_0	u'_e/u_j	grid	n_θ	Tu_j/r_0	data
M09Re1e5TaLd0150v9	0.9	100,000	1	L	0.15	9%	FGz40	1,024	5,500	D0
M09Re5e4Ta1_5Ld0150v9	0.9	50,000	1.5	L	0.15	9%	FGz40	1,024	700	D1
M09Re1e5Ta1_5Ld0150v9	0.9	100,000	1.5	L	0.15	9%	FGz40	1,024	2,500	D1
M09Re2e5Ta1_5Ld0150v9	0.9	200,000	1.5	L	0.15	9%	FGz40	1,024	700	D1
M09Re2_5e4Ta2_25Ld0150v9	0.9	25,000	2.25	L	0.15	9%	FGz40	1,024	700	D1
M09Re1e5Ta2_25Ld0150v9	0.9	100,000	2.25	L	0.15	9%	FGz40	1,024	2,500	D1

Table 13 LES of hot tripped jets at Mach numbers between 0.3 and 1.3; see caption of table 1 for the different parameters.

jet	M	Re_D	T_j/T_a	BL	δ_{BL}/r_0	u'_e/u_j	grid	n_θ	Tu_j/r_0	data
M045Re1e5Ta1_5Ld0150v9	0.45	100,000	1.5	L	0.15	9%	FGz40	1,024	1,200	D1
M06Re1e5Ta1_5Ld0150v9	0.6	100,000	1.5	L	0.15	9%	FGz40	1,024	1,650	D1
M075Re1e5Ta1_5Ld0150v9	0.75	100,000	1.5	L	0.15	9%	FGz40	1,024	1,650	D1
M09Re1e5Ta1_5Ld0150v9	0.9	100,000	1.5	L	0.15	9%	FGz40	1,024	2,500	D1
M11Re1e5Ta1_5Ld0150v9	1.1	100,000	1.5	L	0.15	9%	FGz40	1,024	1,400	D1
M13Re1e5Ta1_5Ld0150v9	1.3	100,000	1.5	L	0.15	9%	FGz50	1,024	1,400	D1
M06Re1e5Ta2_25Ld0150v9	0.6	100,000	2.25	L	0.15	9%	FGz40	1,024	1,200	D1
M075Re1e5Ta2_25Ld0150v9	0.75	100,000	2.25	L	0.15	9%	FGz40	1,024	1,650	D1
M09Re1e5Ta2_25Ld0150v9	0.9	100,000	2.25	L	0.15	9%	FGz40	1,024	2,500	D1
M11Re1e5Ta2_25Ld0150v9	1.1	100,000	2.25	L	0.15	9%	FGz40	1,024	1,400	D1
M13Re1e5Ta2_25Ld0150v9	1.3	100,000	2.25	L	0.15	9%	FGz50	1,024	1,400	D1
M16Re1e5Ta2_25Ld0150v9	1.6	100,000	2.25	L	0.15	9%	FGz50	1,024	300	D1

Table 14 Numbers of points n_r and n_z and extents of the physical domain L_r and L_z in the radial and axial directions, and mesh spacings Δr and Δz at different positions.

					$\Delta r/r_0$ (%) at			$\Delta z/r_0$ (%) at		
grid	n_r	n_z	L_r	L_z	$r=0$	$r=r_0$	$r=L_r$	$z=0$	$z=15r_0$	$z=L_z$
CGz75a	427	2458	$25r_0$	$75r_0$	2.48	0.72	14.94	1.45	2.49	6.25
CGz75b	479	2458	$25r_0$	$75r_0$	2.48	0.72	10.03	1.45	2.49	6.25
CGz90	479	3058	$25r_0$	$90r_0$	2.48	0.72	10.03	1.45	2.49	6.25
FGz40	504	2085	$15r_0$	$40r_0$	1.41	0.36	7.55	0.72	2.30	4.88
FGz50	572	2412	$15r_0$	$50r_0$	1.41	0.36	5.03	0.72	2.12	5.31
FGz60	572	2947	$15r_0$	$60r_0$	1.41	0.36	5.03	0.72	1.82	4.95
FGz70	626	3822	$15r_0$	$70r_0$	1.41	0.36	4.02	0.72	1.47	4

Table 15 Recording files: Strouhal number given by the sampling frequency, recording positions, and variables recorded (density ρ, velocity components $u_i = (u_r, u_t, u_z)$, pressure p, vorticity norm $|\omega|$, dilatation Θ).

files	St_D	z	r	θ	variables
$3Daero$	6.4	$0 \rightarrow 30r_0$ every $2\Delta z$	$0 \rightarrow 6r_0$ every $2\Delta r$	$0 \rightarrow 2\pi - 2\pi/512$ every $2\pi/512$	ρ, u_i, p
$3Dac$	6.4	$0 \rightarrow L_z$ every $2\Delta z$	L_r	$0 \rightarrow 2\pi - 2\pi/512$ every $2\pi/512$	p
	6.4	$0 \rightarrow L_z$ every $2\Delta z$	$0 \rightarrow L_r$ every Δr	$0 \rightarrow 3\pi/2$ every $\pi/2$	p
	6.4	$0 \rightarrow L_z$ every $10r_0$	$0 \rightarrow L_r$ every Δr	$0 \rightarrow 2\pi - 2\pi/512$ every $2\pi/512$	p
R_0	12.8	$-1.25r_0 \rightarrow L_z$ every $2\Delta z$	0	$0 \rightarrow 2\pi - 2\pi/256$ every $2\pi/256$	$\rho, u_i, p, \|\omega\|, \Theta$
R_1	12.8	$-1.25r_0 \rightarrow L_z$ every $2\Delta z$	r_0	$0 \rightarrow 2\pi - 2\pi/256$ every $2\pi/256$	$\rho, u_i, p, \|\omega\|, \Theta$
R_{WP}	12.8	$-1.25r_0 \rightarrow L_z$ every $2\Delta z$	$1.4r_0$ at $z = 0$ 8^o cone angle	$0 \rightarrow 2\pi - 2\pi/256$ every $2\pi/256$	$\rho, u_i, p, \|\omega\|, \Theta$
R_{NF}	12.8	$-1.25r_0 \rightarrow L_z$ every $2\Delta z$	L_r	$0 \rightarrow 2\pi - 2\pi/256$ every $2\pi/256$	ρ, u_i, p
T_{axi}	6.4	$-1.25r_0 \rightarrow L_z$ every Δz	$0 \rightarrow L_r$ every Δr		Fourier coef $n_{\theta=0}$ for ρ, u_i, p
T_{0-270}	6.4	$-1.25r_0 \rightarrow L_z$ every Δz	$0 \rightarrow L_r$ every Δr	$0 \rightarrow 3\pi/2$ every $\pi/2$	$\rho, u_i, p, \partial u_i/\partial\theta$
T_{45-315}	6.4	$-1.25r_0 \rightarrow L_z$ every Δz	$0 \rightarrow L_r$ every Δr	$\pi/4 \rightarrow 13\pi/4$ every $\pi/2$	$\rho, u_i, p, \partial u_i/\partial\theta$
$T_{n_\theta=0-4}$	6.4	$0 \rightarrow L_z$ every $2\Delta z$	$0 \rightarrow L_r$ every $2\Delta r$		Fourier coef $n_{\theta=0\rightarrow4}$ for $\rho, u_i, p, \|\omega\|, \Theta$
$T_{n_\theta=5-8}$	6.4	$0 \rightarrow L_z$ every $2\Delta z$	$0 \rightarrow L_r$ every $2\Delta r$		Fourier coef $n_{\theta=5\rightarrow8}$ for $\rho, u_i, p, \|\omega\|, \Theta$
T_{HF}	32	$0 \rightarrow 20r_0$ every $2\Delta z$	$0 \rightarrow 3.5r_0$ every $2\Delta r$	0	ρ, u_i, p
$Z_{0/start/end}$	12.8	$-1.25r_0, 0, L_z$	$0 \rightarrow L_r$ every Δr	$0 \rightarrow 2\pi - 2\pi/256$ every $2\pi/256$	ρ, u_i, p
Z_{5-35}	6.4	$5r_0 \rightarrow 35r_0$ every $5r_0$	$0 \rightarrow L_r$ every $2\Delta r$	$0 \rightarrow 2\pi - 2\pi/256$ every $2\pi/256$	ρ, u_i, p

Table 16 Set of files recorded in the simulations.

jets	case	files recorded
M09Re1e5TaLd0150v9	D0	all files
most jets at $Re_D \geq 12,500$	D1	all files except for $3Daero$, $3Dac$ and T_{45-315}
jets at $Re_D = 3,125$	D2	all files except for $3Daero$, $3Dac$, T_{45-315}, $T_{n_\theta=5-8}$ and T_{HF}
untripped jets at $M \neq 0.9$	D3	all files except for $3Daero$, $3Dac$, T_{45-315}, $T_{n_\theta=2-8}$, T_{HF} and Z_{5-35}